Asian Journal of Chemistry; Vol. 32, No. 12 (2020), 3239-3248

ASIAN JOURNAL OF CHEMISTRY

https://doi.org/10.14233/ajchem.2020.22972

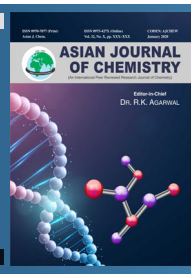

Synthesis and Application of Novel Coal Fly Ash Supported C-Doped TiO_2-SnO_2 Photocatalytic Nanocomposite for the Removal of Dyes in Water

S. Sambakanya[1], P. Nyamukamba[1,2,*], D.M. Katwire[1], H.H. Mungondori[1,3], P. Mukumba[2] and O. Okoh[1]

[1]Department of Chemistry, University of Fort Hare, P. Bag X1314, Alice, 5700, South Africa
[2]Department of Physics, University of Fort Hare, P. Bag X1314, Alice, 5700, South Africa
[3]Department of Applied Sciences, Walter Sisulu University, PO Box 1421, East London, 5200, South Africa

*Corresponding author: Tel: +27 78 4922249; E-mail: pnyamukamba@ufh.ac.za

Received: 28 August 2020; *Accepted*: 23 November 2020; *Published online*: 7 December 2020; AJC-20166

Herein, the preparation, characterization and applications of novel carbon doped titanium dioxide and tin oxide nanocomposite supported on coal fly ash (C-TiO_2-SnO_2/CFA) are reported. The nanocomposite nanoparticles were successfully synthesized by a sol-gel method and calcined at 550 ºC. XRD analysis showed that SnO_2 nanoparticles were polycrystalline in nature and TiO_2 had both anatase and rutile phases. Diffuse reflectance spectra showed that carbon doping reduced the band gap of TiO_2 from 3.19 eV to 2.78 eV. The nanoparticles′ photocatalytic activity was evaluated using methyl orange and methylene blue dyes, under both UV light and solar irradiation at different pH, pollutant concentration and photocatalyst loading. High photodegradation rates of methyl orange were achieved under visible light. The optimum loading of composite photocatalyst was 0.4 g with removal efficiencies of 97.75% for methyl orange and 99.25% for methylene blue after 3 h. High removal efficiencies were achieved for methyl orange at pH 3 and for methylene blue at pH 10.

Keywords: Coal fly ash, Doping, Nanoparticles, Methylene blue, Methyl orange, Photocatalysis, Tin dioxide, Titanium dioxide.

INTRODUCTION

Increased water contamination around the world has highlighted immense recognition of the need for solutions that are friendly towards the environment to eradicate pollutants [1]. High concentrations of dangerous chemical substances that endanger natural water supplies are being released into the environment and these include phenols, phthalates, azo dyes, herbicides and pesticides. The overuse of fertilizers and pesticides, traces of chemical residue and heavy metals all contribute to water pollution [2].

In view of the current water pollution issues, it is necessary to invent new strategies for water treatment and improve the existing techniques so that harmful substances can be effectively removed from natural water before use. Many wastewater treatment methods have been studied and used, but they are no longer sufficient to clean highly polluted water. Several approaches which include flocculation and coagulation, electrochemical oxidation, reverse osmosis and activated carbon adsorption have been recently investigated and have proven not to be sufficient [3]. The major disadvantage of the above approaches is the creation of highly concentrated contaminants/secondary pollutants (sludge) that need proper disposal [4]. Nonetheless, the best methods for reducing persistent organic contaminants to non-toxic end products are advanced oxidation processes (AOPs). Such techniques which include photocatalysis involve the generation of reactive species such as hydroxyl radicals.

This innovative research aims to use coal fly ash supported C-TiO_2/SnO_2 as a photocatalyst in the photodegradation of organic pollutants in water. Titanium dioxide, a naturally occurring oxide of titanium, has a variety of uses which includes pigment in paint and colouring of food. It is the most widely used photocatalyst in photocatalysis because it is cheap, easily available, corrosion resistant, environmental friendly and relatively stable over a wide pH range, relatively easy to produce and use, relatively non-toxic, its photogenerated holes are highly oxidizing and has a relatively low rate of charge carrier recombination compared to other semiconductors [5,6]. On the other hand, tin oxide (SnO_2) is an amphoteric, colourless solid, also

known as cassiterite. It is an n-type semiconductor with a large band gap of 3.6 eV at room temperature, high optical clarity and reflectivity with strong chemical and thermal stability in the infrared region [7]. Because of these characteristics, tin oxide was considered for use in infrareds and optoelectronic devices, as a catalyst and raw material for transparent films [8]. The highly oxidizing properties also make it an effective photocatalyst for removing contaminants from water.

TiO_2 and SnO_2 are the most commonly utilized photocatalysts for research and industrial purposes. Besides all the good properties which are displayed by these photocatalysts, there are some shortcomings involving their use. The major issues of using pure TiO_2 and SnO_2 are the wide band gaps and high recombination rates of the electron hole pairs which have an effect on the interfacial charge transfer processes leading to a low photon quantum efficiency of the photocatalytic process [9]. TiO_2 absorbs in the ultraviolet region (< 365 nm), which is only about 5% of the total solar radiation and this implies that more energy requires to supply light of appropriate wavelength, thus making the use of TiO_2 expensive [10]. Hence, there is a need to modify TiO_2 and SnO_2, so that they can absorb in the visible region, which is the major part of the solar radiation (43%).

The major aim of this study was to prepare coal fly ash supported C-TiO_2-SnO_2 photocatalytic composite that is active in visible light for the treatment of water. Coal fly ash (CFA) will act as a support for the photocatalyst to allow easy recovery of the photocatalyst after photodegradation. It is also a good low cost adsorbent for heavy metals and dyes, which allows simultaneously removal of heavy metals and dyes. The enhanced photocatalytic activity of C-TiO_2-SnO_2/CFA photocatalyst will enable rapid and efficient removal of contaminants in water. This offers an environmental friendly and potentially cost-effective water treatment method that can help reduce the cost of delivering water especially to the poorest communities of developing countries.

EXPERIMENTAL

The chemicals used in the preparation of C-TiO_2-SnO_2/CFA were titanium(IV) butoxide (97%, Sigma-Aldrich), while methanol (99.5%) was used as precursors in the preparation of TiO_2. Tin(IV) chloride (99%, Merck) and citric acid were used as precursors in the preparation of SnO_2. Ammonia solution (25%, NH_4OH) was used to adjust pH. Ethanol (99.9%, Merck) and distilled water were used as solvents. Glucose (Merck, Germany) was used as a carbon source in doping TiO_2. Methyl orange and methylene blue (Merck) were used as model organic pollutants in the photodegradation studies. Hydrochloric acid (32%) and ammonia (25%) were used to adjust pH of the organic pollutants. Coal fly ash was supplied by Eskom South Africa's coal fired power stations.

Characterization: XRD patterns of the specimens were recorded on a Bruker D8 Discover, fitted with a proportional counter, using Cu-Kα diffraction radiation (λ =1.5405 level, nickel filter). Fourier transform infrared (FTIR) spectra were acquired on a Perkin-Elmer FTIR Spectrum 200 spectrophotometer. Diffuse reflectance spectra (DRS) of the samples were obtained using a diffuse reflectance attachment of a Cary 500 UV-Vis-NIR spectrophotometer the range 800 nm to 200nm at room temperature. UV-Vis spectra of the pollutants were obtained on a Perkin-Elmer Lambda 365 UV-Vis spectrometer.

Purification of coal fly ash (CFA): The coal fly ash was purified following a procedure reported by Visa and Duta [11]. About 100 g CFA was mixed with 1000 mL of ultrapure water and stirred for 48 h at room temperature (20-22 ºC) until a constant pH and conductivity was achieved to eliminate the soluble compounds. The resulting material was filtered, washed and dried between 105 and 115 ºC until a constant mass was attained. The resulting substrate was then sieved.

Preparation of coal fly ash (CFA) supported SnO_2: A modified version of the method by Shide *et al.* [12] was used to prepare SnO_2/CFA composite nanoparticles. In a typical experiment, $SnCl_4$ and citric acid with a mole ratio of 2:1 were added in a beaker containing distilled water with magnetic stirring. The pH of the resulting solution was adjusted to 1.5 using NH_4OH. The resulting white gel was stirred for about 2 h, followed by addition of coal fly ash. The nanoparticles were separated from the solution by centrifugation, washed thoroughly with distilled water to remove excess Cl^-, dried at 50 ºC in an oven and finally calcined at 600 ºC for 2 h in a furnace.

Preparation of pure SnO_2: Undoped SnO_2 nanoparticles were also prepared *via* the sol gel synthesis method. The procedure that was employed is similar to that used in the preparation of SnO_2 supported on coal fly ash, except for the addition of coal fly ash.

Preparation of carbon doped TiO_2: Carbon doped titanium dioxide (C-TiO_2) nanoparticles were prepared by the hydrolysis of titanium(IV) butoxide using a modified method as reported by Behnajady *et al.* [13]. In a typical experiment, titanium(IV) butoxide and methanol were mixed in a round bottom flask, then placed in a sonic bath for 15 min at 25 ºC, followed by addition of water and refluxing at 80 ºC for 30 min. Glucose was then added to the reaction mixture as a carbon source and then refluxing was continued for 150 min. The resulting sol was separated from the solution by centrifugation, dried at 60 ºC in an oven and calcined at 550 ºC for 2 h in a furnace.

Preparation of undoped TiO_2: Undoped TiO_2 nanoparticles were also prepared using the same method used in the preparation of C-TiO_2, except for the addition of a dopant. The preparation of undoped TiO_2 was necessary for comparison purposes.

Preparation of C-TiO_2-SnO_2/CFA: The coal fly ash supported carbon doped TiO_2 and SnO_2 nanoparticles were prepared using a modified sol gel method as defined by Behnajady *et al.* [13]. The procedures that were employed were similar to those used in the preparation of C-TiO_2. Similarly, in a typical experiment, titanium(IV) butoxide and methanol were put in a three necked round bottom flask. The solution was put in a sonic bath for 15 min at 25 ºC, followed by addition of water and refluxed at 80 ºC. After 30 min of refluxing, glucose was added as a carbon source and an hour later SnO_2/CFA was added to the solution and kept under vigorous stirring at 80 ºC and refluxed for a total of 150 min. The resulting sol was separated

via centrifugation, dried at 60 ºC in an oven and calcined at 550 ºC for 2 h in a furnace.

Photocatalytic activity: A sample of C-TiO_2-SnO_2/CFA composite (0.4 g) was placed in a reaction vessel containing 50 mL of 20 ppm methyl orange. This was then irradiated with UV light of wavelength 366 nm with magnetic stirring. Another experiment using the same photocatalyst was also done under visible light and all the experiments were performed in triplicate. All the experiments were carried out at 25 ºC and pH 7 except in the cases, where the effect of pH was investigated. Aliquots were taken at 30 min intervals for a period of 3 h and analyzed by UV-Vis spectrometer at a wavelength of 460 nm for methyl orange and 665 for methylene blue.

RESULTS AND DISCUSSION

FTIR studies: FT-IR was used to identify the functional groups of the prepared photocatalysts. Fig. 1a shows the FT-IR spectra of SnO_2, SnO_2/CFA and CFA. The broad peaks around 600 cm^{-1} in the spectra of both SnO_2 and SnO_2/CFA are due to Sn-O modes of Sn-O-Sn [14]. The broad peak around 1100 cm^{-1} in the spectrum of CFA was assigned to the Si-O-Si and Si-O-Al anti-symmetric stretching vibrations, which tend to shift to 1600 cm^{-1} in the spectrum of SnO_2/CFA. From this observation, it can be assumed that the appearance of this peak was caused by the presence of CFA in the TiO_2 photocatalysts. The peak around 1600 cm^{-1} in the spectrum of CFA and SnO_2/CFA spectra is assigned to the stretch vibration mode and characteristic bending frequency of O-H groups of adsorbed water [15].

The two absorption bands found at 3300 and 1650 cm^{-1} in the spectra of TiO_2, 4% C-TiO_2 and 4% C-TiO_2-SnO_2/CFA (Fig. 1b) are the characteristic of the OH bending modes due to adsorbed water and hydroxyl groups [16]. The peak appearing around 750 cm^{-1} in all the spectra is attributed to Ti-O-Ti bending vibrations of TiO_2. The peaks between 1140 and 1100 cm^{-1} in both the spectra of C-TiO_2 and C-TiO_2-SnO_2/CFA are due to C-O stretching [17]. The peak around 1670 cm^{-1} in all the FTIR spectra in Fig. 1b is due to Ti-OH bending modes. The broad peaks located around 600 cm^{-1} in the spectrum of 4% C-TiO_2-SnO_2/CFA is due to Sn-O modes of Sn-O-Sn [14].

SEM studies: The prepared C-TiO_2-SnO_2/CFA composites were also analyzed by SEM to study their surface morphology. It was observed that the individual particles of SnO_2 exhibit a nearly round shape and were of variable sizes (Fig. 2a). The surface morphology of SnO_2 changed with the addition of CFA, from the semi-round nanoparticles to scattered angular particles with large surface area. It can be clearly seen in Fig. 2 that the particles of SnO_2 exhibit a roughly spherical spongy shape, while the particles of SnO_2/CFA exhibit angular shape. The nanoparticles of C-TiO_2 also exhibit a semi round shape whereas the nanoparticles of C-TiO_2-SnO_2/CFA exhibit a quasi-spherical shape. The nanoparticles of C-TiO_2 show that there was agglomeration that occurred.

TEM studies: Transmission electron microscopy was also used to determine the particle size of the samples. TEM images of TiO_2, C-TiO_2, SnO_2 and C-TiO_2-SnO_2/CFA are shown in Fig. 3. The average particle size of SnO_2 was found to be 19.98 nm which is closer to the value of 18.43 nm calculated using the Schererr equation using XRD data. The particle size of pure TiO_2 was 16.19 nm whereas that of doped TO_2 was found to have particle size of about 14.84 nm, which implying that doping resulted in reduction of particle size. The particle sizes from TEM images are slightly different to those calculated from

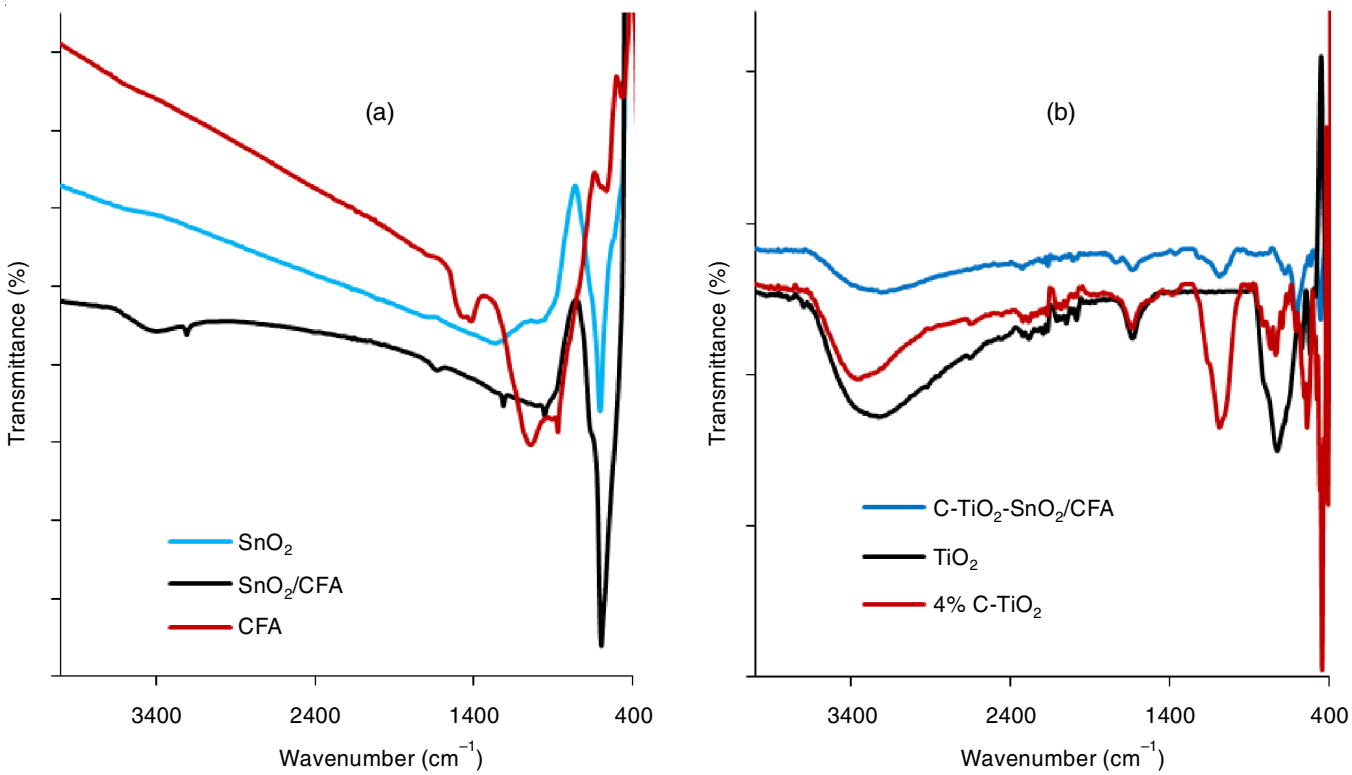

Fig. 1. (a) FTIR spectrum of SnO_2, SnO_2/CFA, CFA and (b) TiO_2, 4%C-TiO_2 and 4% C-TiO_2-SnO_2/CFA

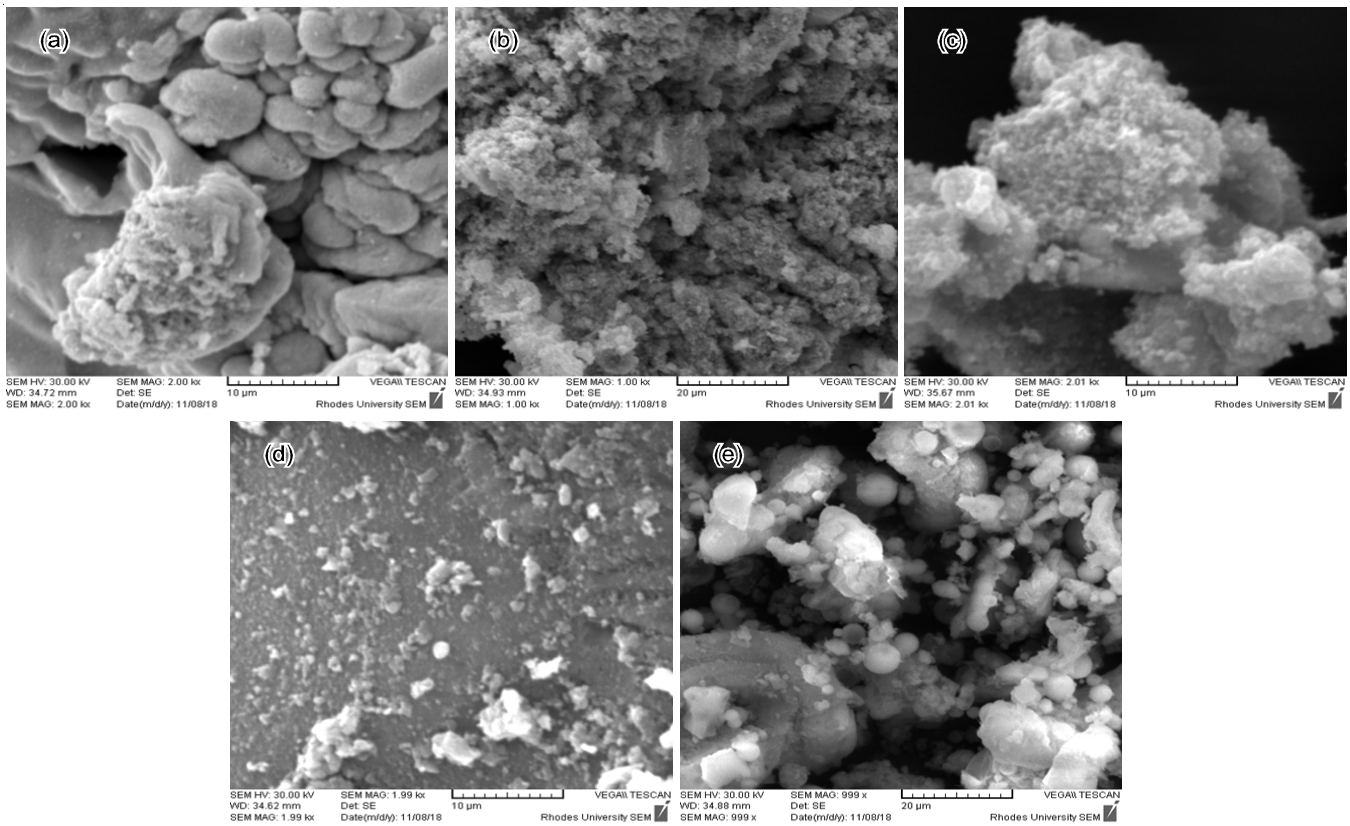

Fig. 2. SEM images of (a) SnO_2, (b) SnO_2/CFA, (c) C-TiO_2 and (d) C-TiO_2-SnO_2/CFA and (e) CFA

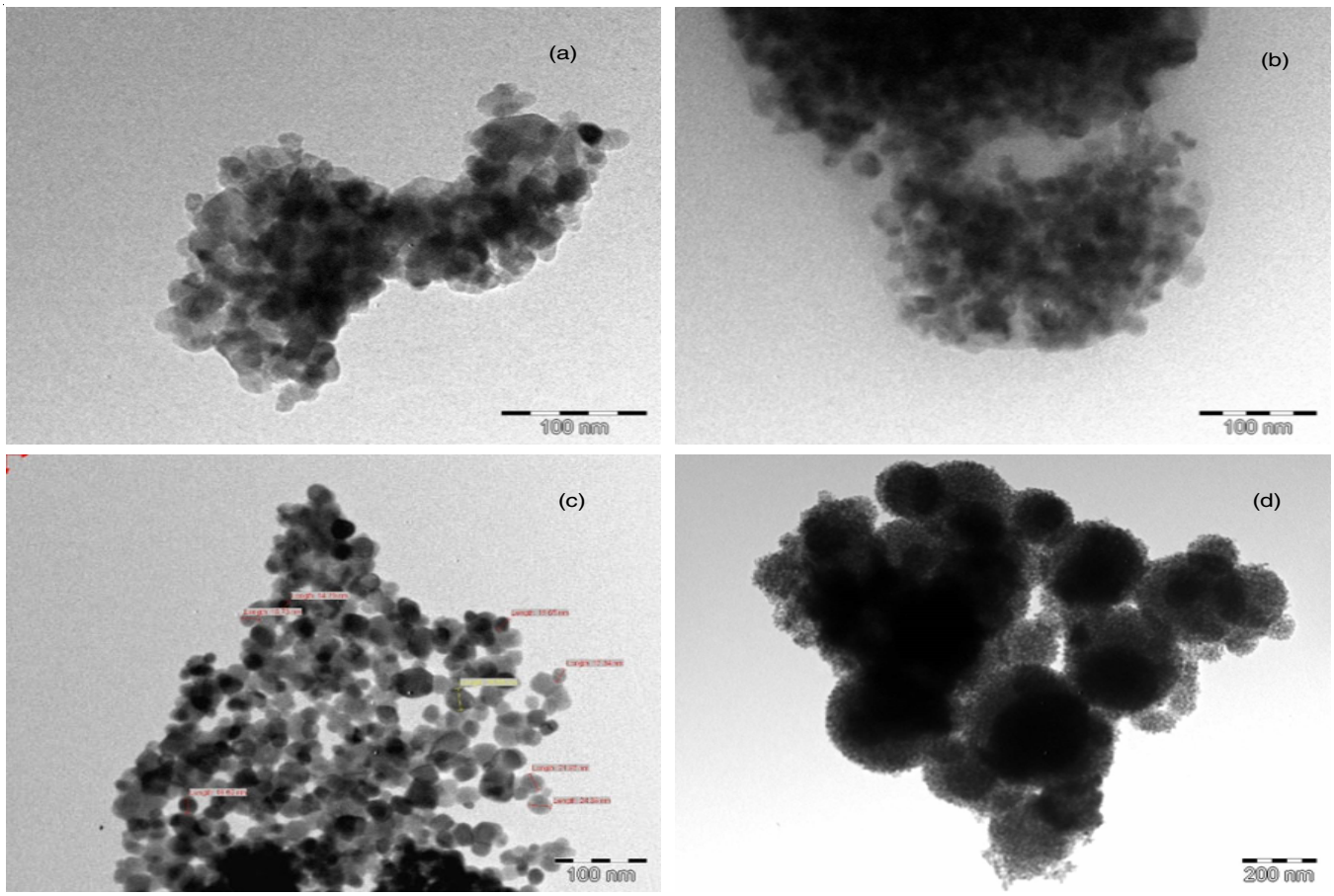

Fig. 3. TEM images of (a) TiO_2, (b) C-TiO_2, (c) SnO_2 & (d) C-TiO_2-SnO_2/CFA

XRD, which is expected since the results of the calculations were obtained from different instruments [18]. The change in size of the particles of the composite was significant as seen on the TEM images.

XRD studies: The XRD analysis was used to determine the crystalline nature and estimate the particle size of C-TiO_2-SnO_2/CFA composite nanoparticles. In the XRD pattern of TiO_2 (Fig. 4a) and 4% C-TiO_2 (Fig. 4b), the peaks at 2θ values of 25.2°, 31.0°, 37.8°, 48.3°, 54.0°, 63.5°, 68.0°, 70.0°, 75.2° and 83.0° are due to the anatase phase of TiO_2 while the peak at 2θ value of 27° is due to the rutile phase. The sharp peaks that were found in the XRD pattern of C-TiO_2 were sharper and more intense than the peaks that were found in the XRD pattern of pure TiO_2, indicating that the as-prepared C-TiO_2 were more crystalline than undoped TiO_2. This clearly shows that there were changes brought about by doping.

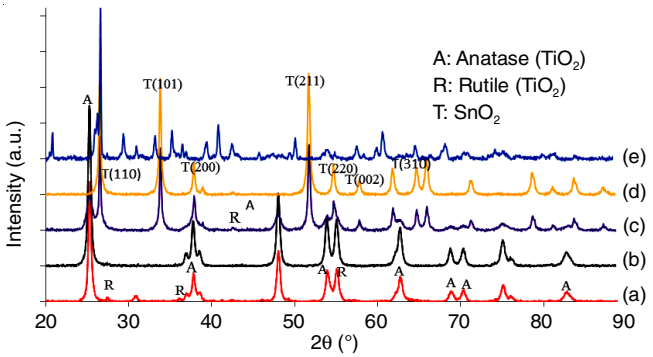

Fig. 4. XRD patterns of (a) TiO_2, (b) 4% C-TiO_2, (c) 4% C-TiO_2-SnO_2/CFA, (d) SnO_2 and (e) CFA

The diffraction peaks at 2θ values of 20° and 26° in the XRD pattern of CFA (Fig. 4e) indicates the presence of quartz and berlinite in CFA. The peaks at 2θ values of 28° and 31° indicate the presence of dolomite and that at 2θ value of 29° indicates the presence of calcite in the CFA [19]. In the XRD pattern of SnO_2 (Fig. 4d), the peaks at 2θ values 37.8°, 51.0°, 54.0°, 57.0°, 62.0°, 65.0°, 71.0° and 78.0° indicate the polycrystalline nature of SnO_2 nanoparticles [20]. The XRD pattern show diffraction peaks for the orthorhombic structure of SnO_2 appeared (JCPDS file No. 78-1063). In the XRD pattern of 4% C-TiO_2-SnO_2/CFA composite (Fig. 4c), the peak at 2θ value of 26° indicates the presence of CFA in the 4% C-TiO_2-SnO_2/CFA. The peaks found at 2θ values of 25.2°, 37.0° and 48.0° were due to TiO_2 in the anatase phase and the peak at 2θ values of 26.5°, 31.0°, 54.0° and 62.7° were due to TiO_2 in the rutile phase. The peaks at 2θ values of 26.5°, 33.0°, 37.8.0°, 51.5.0°, 54.0°, 57.0°, 62.8.0°, 65.0° and 78.0° indicate the presence of polycrystalline SnO_2 nanoparticles in the XRD pattern of 4% C-TiO_2-SnO_2/CFA composite [21].

The particle size of SnO_2, TiO_2 C-TiO_2 and 4% C-TiO_2-SnO_2/CFA were calculated using the Scherrer equation (eqn. 1) and the sizes were found to be 18.43, 14.50, 13.98 and 14.44 nm, respectively.

$$\tau = \frac{k\lambda}{\beta\cos\theta} \quad (1)$$

To estimate the percentage of anatase (A%) in the composite, eqn. 2 was used for calculations [22].

$$A\ (\%) = \frac{100}{\left(1+1.265\frac{I_r}{I_a}\right)} \quad (2)$$

where I_r is the peak intensity of rutile at 2θ value of 26.5° and I_a is the peak intensity of anatase at 2θ value of 25.2°.

The amount of rutile that was transformed as a mass fraction (FR) was calculated using eqn. 3 [22]:

$$FR\ (\%) = \frac{1}{\left(1+0.79\frac{I_a}{I_r}\right)} \quad (3)$$

where I_a is the integrated intensity of anatase (2θ = 25.3°) and I_r is the integrated intensity of rutile (2θ = 26.7°). Using the above equation the percentage of anatase in the composite was found to be 43.19% and that of rutile 56.83%.

DRS analysis: Diffuse reflectance spectroscopy analysis was used to determine the band gap energy of the prepared photocatalysts. The band gap energy of the samples was estimated using Kubelka and Munk's theory in accordance with the following equation:

$$F(R) = \frac{(1-R)^2}{2R} \quad (4)$$

where F(R) is Kubelka-Munk's function and R is the reflectance [23].

The diffuse reflectance spectra of carbon doped TiO_2-SnO_2 composites is shown in Fig. 5. The undoped TiO_2 had a bandgap of 3.19 eV while C-TiO_2 exhibited a band gap of 2.78 eV, showing that the doping process reduced the band gap of TiO_2. The band gaps of TiO_2-SnO_2 and C-TiO_2-SnO_2/CFA were 3.16 eV and 2.91 eV, respectively. The results obtained shows the coupling of TiO_2 with SnO_2 had a small effect on band gap energy reduction (from 3.19 eV to 3.16 eV); however, it had an effect on the performance of the photocatalyst. C-TiO_2-SnO_2/CFA also exhibited a reduced band gap energy of 2.91 eV. This reduced band gap is an advantage as low energy is required to excite an electron from the valence band to the conduction band band.

Photocatalytic activity

Effect of carbon doping on the photodegradation of methyl orange: The photodegradation efficiencies of TiO_2 doped with different percentages of carbon were evaluated using methyl orange solution under visible light irradiation. The photodegradation curves of methyl orange using TiO_2 photocatalyst doped with 2%, 4% and 6% carbon are shown in Fig. 6. The highest photodegradation was achieved by using TiO_2 photocatalyst doped with 4% carbon. The removal efficiencies of 84.4%, 96.25% and 96.65% were obtained after 3 h under visible irradiation using 2%, 4% and 6% C-TiO_2 photocatalyst, respectively. When the percentage of doping was increased from 2% to 4%, a steady increase was detected in the degradation of methyl orange. However, when the percentage of carbon doping rose to 6%, the rate of degradation of methyl orange did not change significantly. This may be due to excess

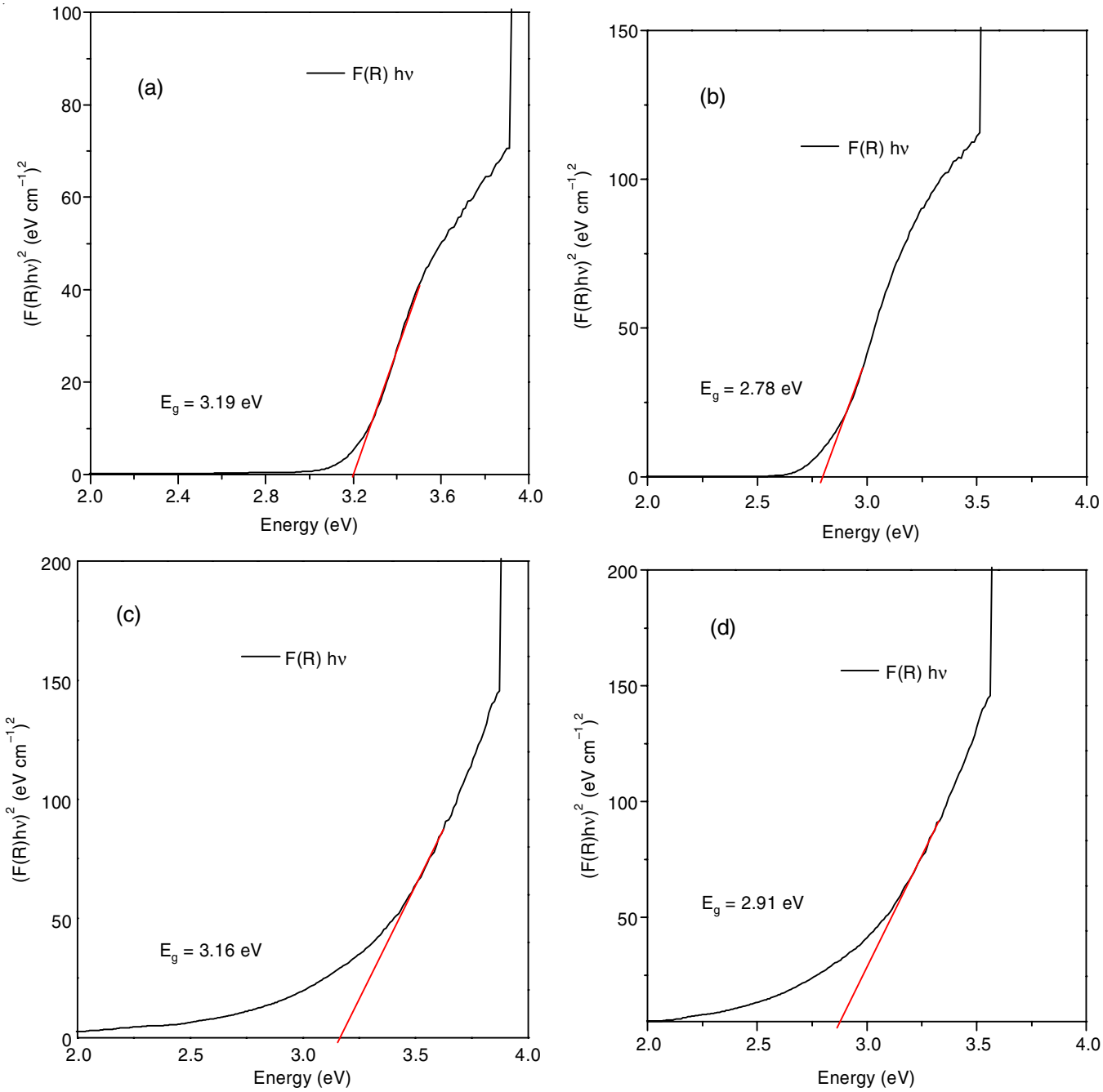

Fig. 5. DRS curves of (a) TiO_2, (b) C-TiO_2 (c) TiO_2-SnO_2 and (d) C-TiO_2-SnO_2/CFA

dopant that can act as recombination centers thus facilitating the recombination of electron-hole pairs. The results of this study show that the optimum carbon loading was 4% hence this photocatalyst was used in further investigations in other experiments.

Effect of photocatalyst loading: The effect of photocatalyst loading on methyl orange and methylene blue photodegradation under visible light was investigated using different amounts of C-TiO_2-SnO_2/CFA composite photocatalyst. The photodegradation profiles obtained for methyl orange and methylene blue are shown in Fig. 7. About 97.75% of methyl orange was degraded after 180 min of exposure to visible light using 0.4g of the photocatalyst but when methylene blue was used as a pollutant, 99.25 % was degraded (Fig. 7b). Similar results were also obtained by Nguyen *et al*. [24] using palladium doped TiO_2 photocatalysis where methylene blue removal was higher than that of methyl orange. The rate of photodegradation of methyl orange and methylene blue increased when photocatalyst loading was increased from 0.1 g to 0.4 g. An increase in photcatalyst loading and synergistic effects of TiO_2 and SnO_2 were the reasons for the increase in photodegradation rate [25].

Effect of pH: The effect of pH on the photodegradation of methyl orange and methylene blue was also studied. The photodegradation experiments were performed at pH 3, 7 and 10. In this investigation, the optimal photocatalyst load (0.4 g C-TiO_2-SnO_2/CFA) was used under visible light.

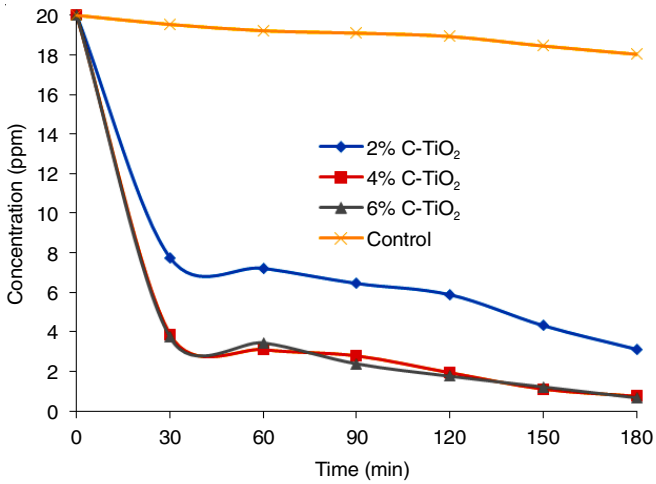

Fig. 6. Photodegradation profiles of methyl orange in water using the control (undoped TiO_2), 2%, 4% and 6% C-TiO_2 photocatalysts at 25 °C and pH 7

Fig. 8 shows the photodegradation curves of methyl orange and methylene blue under acidic, neutral and basic media. In some studies conducted by other researchers, pH is considered as the main parameter, which plays an important role in the degradation of organic pollutants due to its impact on the surface charge of the photocatalyst. Under acidic conditions, methyl orange shows high rates of photodegradation compared to methylene blue as shown in Fig. 8. This is due to the fact that at low pH, the surface of C-TiO_2-SnO_2/CFA photocatalyst is cationic, hence it favours the adsorption of methyl orange which is more negative than methylene blue. The other reason for high degradation rates at low pH could be that the pH was below the point of zero charge hence adsorbent is positive. The removal efficiencies of 95.5% and 92.5% were observed for methyl orange and methylene blue, respectively at pH 3.0. When pH was increased to 7.0 (Fig. 8), the removal efficiencies of methyl orange and methylene blue also increased to 97.75% and 99.25%, respectively. When the pH was increased to 10, methylene blue removal efficiency of 94.35% was observed. Under basic conditions, the rate of photooxidation of methylene blue decreased, indicating that the optimum pH for their photooxidation is around pH 7.0. This is probably due to the value of the point of zero charge on the surface of catalyst at upper pH, which causes the electrostatic aversion between photocatalyst and the dye [26]. Similar results were also found by other researchers who investigated methylene blue degradation under acidic and basic conditions using Cu-TiO_2 [27]. This shows that adjusting the pH of a solution is very crucial in achieving high removal efficiency of organic pollutants in water.

Effect of initial pollutant concentration: The photodegradation efficiency of 0.4g C-TiO_2-SnO_2/CFA was also evaluated using methyl orange and methylene blue solutions with three different initial pollutant concentrations (20, 40 and 60ppm). Fig. 9 shows the methyl orange and methylene blue removal efficiency (RE) curves obtained which were calculated using eqn. 5:

$$RE\ (\%) = \frac{C}{C_o} \times 100 \quad (5)$$

where C is the concentration at any given time; and C_o is the initial concentration of the pollutant.

When the initial concentration was 20 ppm, the removal efficiencies of methyl orange and methylene blue were high

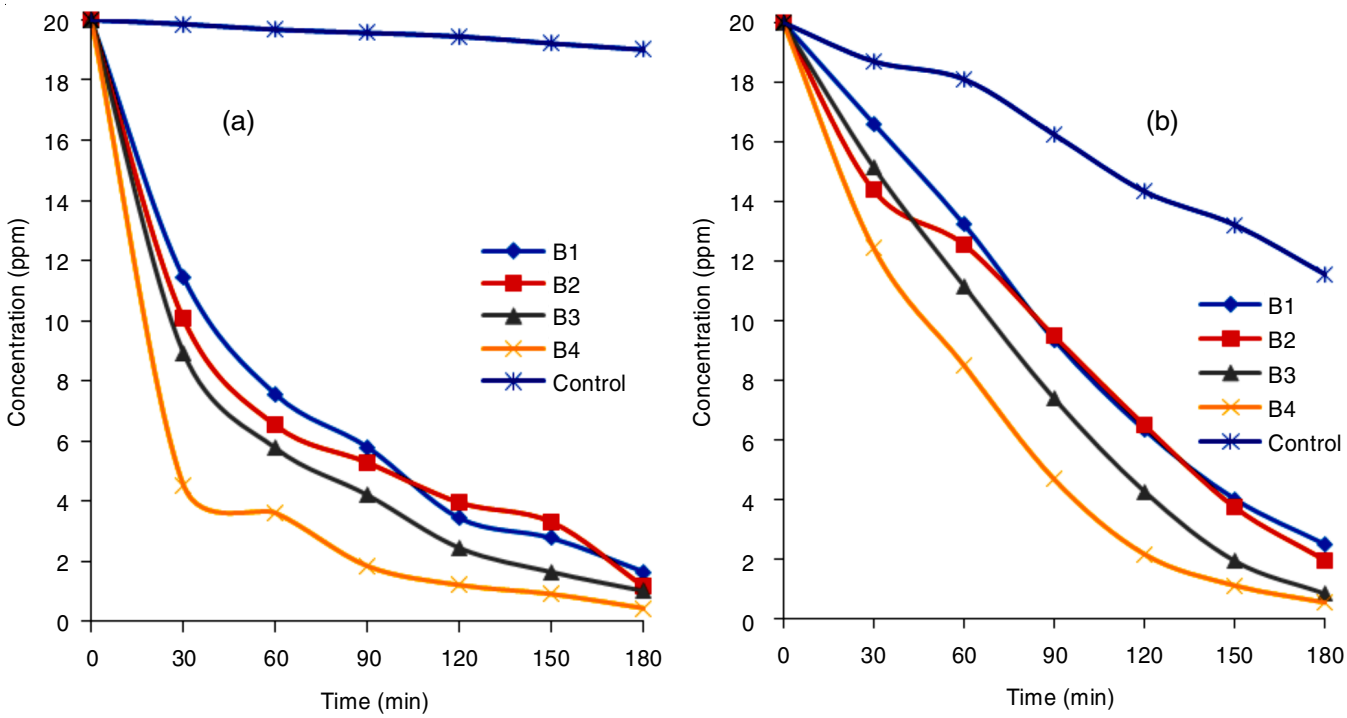

Fig. 7. Photodegradation curves of (a) methyl orange and (b) methylene blue using different amounts of C-TiO_2-SnO_2/CFA photocatalyst at 25 °C and pH 7

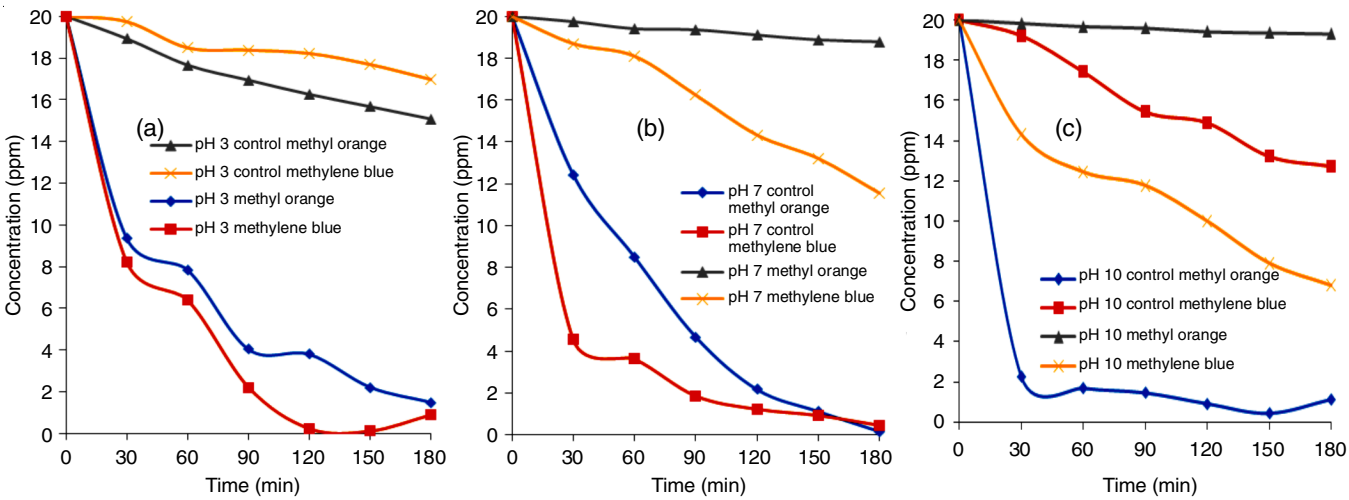

Fig. 8. Photodegradation curves of methyl orange and methylene blue in water at (a) pH 3, (b) pH 7 and (c) pH10.0 and a temperature of 25 °C, under solar irradiation

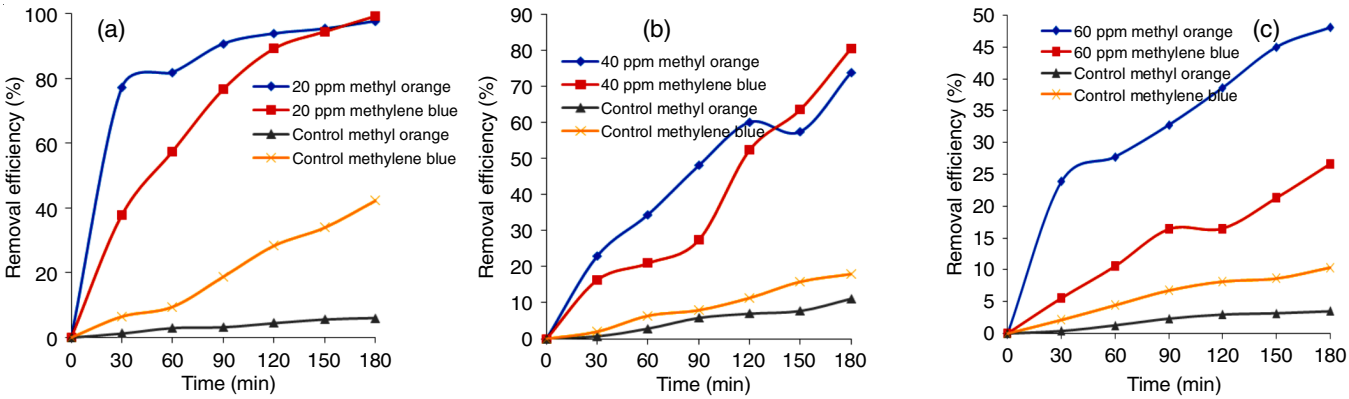

Fig. 9. Photodegradation profiles of methyl orange and methylene blue at (a) 20 ppm, (b) 40 ppm and (c) 60 ppm at pH 7, 25 °C, under visible light using 0.4g C-TiO_2-SnO_2/CFA photocatalyst

as compared to when the concentrations were 40 and 60 ppm. At 20 ppm, methyl orange and methylene blue initial concentration, the removal efficiencies of 99.25% and 97.75% were achieved for methylene blue and methyl orange, respectively. It was observed that methylene blue and methyl orange removal efficiencies decrease by increasing the initial concentration. Similar results were obtained by Çifçiand Meric [28], when they used Ag doped TiO_2 in the decolourization of methylene blue and methyl orange. The results showed that high methylene blue decolourization was observed at low concentration than at high concentrations. High methylene blue concentrations cause a reduction of light penetration into solution and hinder photogeneration of holes. Also, increasing initial concentration of organic pollutant decreases the number of photons or path length of photon that is absorbed on the surface of photocatalyst, which then reduces the excitation of electron from valance band to conduction band. This results in the reduction of photocatalytic activity of the photocatalyst.

Effect of light source: The effect of the light source on the photodegradation of methylene blue in water was also investigated under strict UV_{366} light and under visible light. The optimum photocatalyst loading of 0.4g C-TiO_2-SnO_2/CFA was used with an initial concentration of 20 ppm at 25 ºC and pH 7 for methyl orange and pH 10 for methylene blue. Fig. 10 shows the photodegradation curves obtained under UV and sunlight. It was observed that the degradation of methyl orange and methylene blue was high under visible light than under UV light. The removal efficiencies of 97.75 % and 99.25 % were obtained under visible irradiation after 180 min for methyl orange and methylene blue, respectively. These values are higher than removal efficiencies of 4.5% methyl orange and 92.7% methylene blue that were obtained under UV irradiation after 180 min using the same photocatalyst.

When the percentage photodegradation of C-TiO_2-SnO_2/CFA is compared with other composites from the previous studies, it can be seen that its efficiency is higher as shown in Table-1. The improvement in the photodegradation is due to the narrowing of the band gap thus enhancing the absorption of visible light. Similar results were also obtained by Wang *et al.* [37] when they used iron(III)-doped TiO_2 nanopowders on the photocatalytic degradation of methyl orange under UV and visible light. Their results also showed higher photodegradation of methyl orange under visible light than under UV light [37].

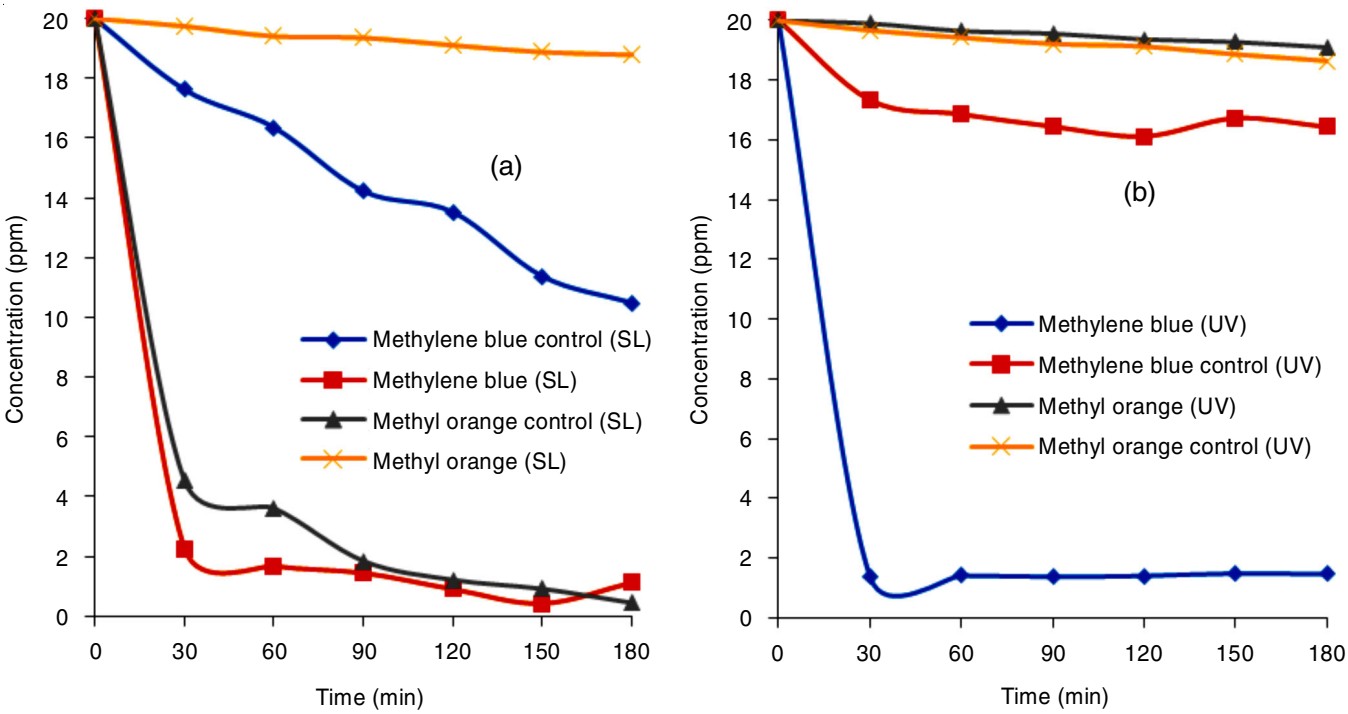

Fig. 10. Photodegradation of methyl orange and methylene blue in water at pH 10, 25 °C, (a) under sunlight (SL) and (b) UV light

TABLE-1
PERCENTAGE PHOTODEGRADATION OF C-TiO_2-SnO_2/CFA AND OTHER COMPOSITES FROM OTHER STUDIES

Pollutants	Composite	Degradation (%)	Ref.	C-TiO_2-SnO_2/CFA (%degradation)
Methylene blue	ZnO–SnO_2	96.53	[29]	99.25
	Fe_2O_3–SnO_2/BC	95.00	[30]	
	SnO_2/$BiVO_4$	72.00	[31]	
	TiO_2/Na-g-C_3N_4	90.00	[32]	
Methyl orange	Bi_2O_3/F–TiO_2	95.00	[33]	97.75
	GO–TiO_2–ZnO	57.70	[34]	
	GO/TiO_2	90.00	[35]	
	SnO_2 aerogel/rGO	84.00	[36]	

Conclusion

FTIR analysis indicated the presence of expected functional groups and the images obtained from SEM revealed that carbon doped titanium dioxide and tin oxide nanocomposite supported on coal fly ash (C-TiO_2-SnO_2/CFA) were quasi-spherical in shape. The XRD patterns revealed successful synthesis of C-TiO_2-SnO_2/CFA composite with polycrystalline rutile phase and anatase phase. The doping of TiO_2 and SnO_2 proved to be a promising way of enhancing the photocatalytic activity of the photocatalyst through the reduction of the band gap, which allowed utilization of visible light. Higher photodegradation rates of methyl orange and methylene blue were achieved under visible light compared to UV light. The photodegradation rates were found to increase with an increase in photocatalyst loading. The optimal loading of carbon dopant for better photocatalytic activities was found to be 4% and the highest removal efficiencies of 97.75% and 99.25% were achieved for methyl orange and methylene blue, respectively. High removal efficiencies were achieved for methyl orange at pH 3 and for methylene blue at pH 10. The photodegradation rates were also found to decrease with an increase in initial concentration.

ACKNOWLEDGEMENTS

The authors are thankful to Sasol Inzalo Foundation and National Research Foundation (NRF) for the funding.

CONFLICT OF INTEREST

The authors declare that there is no conflict of interests regarding the publication of this article.

REFERENCES

1. M. Visa, L. Isac and A. Duta, *J. Appl. Surf. Sci.*, **339**, 62 (2015); https://doi.org/10.1016/j.apsusc.2015.02.159
2. J.Q. Jiang, Z. Zhou and V. Sharma, *J. Microchem.*, **110**, 292 (2013); https://doi.org/10.1016/j.microc.2013.04.014
3. A.M.K. El-ghonemy, *Renew. Sustain. Energy Rev.*, **18**, 6 (2013); https://doi.org/10.1016/j.rser.2012.09.022
4. P.Y. Chan, M. Gamal El-Din and J.R. Bolton, *Water Res.*, **46**, 5672 (2012); https://doi.org/10.1016/j.watres.2012.07.047
5. M. Tahir and N.S. Amin, *J. Appl. Cat. Buss. Environ.*, **162**, 98 (2015); https://doi.org/10.1016/j.apcatb.2014.06.037
6. P. Nyamukamba, L. Tichagwa, J.C. Ngila and L. Petrik, *J. Photochem. Photobiol. Chem.*, **343**, 85 (2017); https://doi.org/10.1016/j.jphotochem.2017.04.014
7. K. Bouras, J.L. Rehspringer, G. Schmerber, H. Rinnert, G. Ferblantier, S. Colis, M. Balestrieri, D. Ihiawakrim, A. Dinia and A. Slaoui, *J. Mater. Chem.C*, **2**, 8235 (2014); https://doi.org/10.1039/C4TC01202J
8. K. Anandan and V. Rajendran, *Superlatt. Microstruct.*, **85**, 185 (2015); https://doi.org/10.1016/j.spmi.2015.05.031
9. G. Sanzone, M. Zimbone, G. Cacciato, F. Ruffino, R. Carles, V. Privitera and M.G. Grimaldi, *Superlatt. Microstruct.*, **123**, 394 (2018); https://doi.org/10.1016/j.spmi.2018.09.028

10. M.B. Suwarnkar, R.S. Dhabbe, A.N. Kadam and K.M. Garadkar, *Ceram. Int.*, **40**, 5489 (2014); https://doi.org/10.1016/j.ceramint.2013.10.137
11. M. Visa and A. Duta, *Chem. Eng. J.*, **223**, 860 (2013); https://doi.org/10.1016/j.cej.2013.03.062
12. S. Wu, C. Li, W. Wei, H. Wang, Y. Song, Y. Zhu and L. Lu, *J. Rare Earths*, **28(Suppl. 1)**, 171 (2010); https://doi.org/10.1016/S1002-0721(10)60313-4
13. M.A. Behnajady, H. Eskandarloo, N. Modirshahla and M. Shokri, *Desalination*, **278**, 10 (2011); https://doi.org/10.1016/j.desal.2011.04.019
14. Z. Luo, Y. Zhu, E. Liu, T. Hu, Z. Li, T. Liu and L. Song, *Mater. Res. Bull.*, **60**, 105 (2014); https://doi.org/10.1016/j.materresbull.2014.08.022
15. T.M. Mokgehle, H. Richards, L. Chimuka, W.M. Gitari and N.T. Tavengwa, *Miner. Eng.*, **141**, 105851 (2019); https://doi.org/10.1016/j.mineng.2019.105851
16. A. Samadi, R. Ahmadi and S.M. Hosseini, *Org. Electron.*, **75**, 105405 (2019); https://doi.org/10.1016/j.orgel.2019.105405
17. N.U.M. Nor and N.A.S. Amin, *J. CO_2 Utilization*, **33**, 372 (2019); https://doi.org/10.1016/j.jcou.2019.07.002
18. S. Varnagiris, A. Medvids, M. Lelis, D. Milcius and A. Antuzevics, *J. Photochem. Photobiol. A*, **382**, 111941 (2019); https://doi.org/10.1016/j.jphotochem.2019.111941
19. Y. Zheng, L. Ke, D. Xia, Y. Zheng, Y. Wang, H. Li and Q. Li, *Sep. Purif. Technol.*, **163**, 282 (2016); https://doi.org/10.1016/j.seppur.2016.01.052
20. G.D. Khuspe, S.T. Navale, M.A. Chougule, S. Sen, G.L. Agawane, J.H. Kim and V.B. Patil, *Synth. Met.*, **178**, 1 (2013); https://doi.org/10.1016/j.synthmet.2013.06.022
21. A. Kusior, L. Zych, K. Zakrzewska and M. Radeck, *Appl. Surf. Sci.*, **471**, 973 (2019); https://doi.org/10.1016/j.apsusc.2018.11.226
22. P. Nyamukamba, L. Tichagwa, S. Mamphweli and L. Petrik, *Int. J. Photoenergy*, **2017**, 3079276 (2017); https://doi.org/10.1155/2017/3079276
23. I. Fatimah, N.I. Prakoso, I. Sahroni, M.M. Musawwa, Y.L. Sim, F. Kooli and O. Muraza, *Heliyon*, **5**, e02766 (2019); https://doi.org/10.1016/j.heliyon.2019.e02766
24. C.H. Nguyen, C.C. Fu and R.S. Juang, *J. Clean. Prod.*, **202**, 413 (2018); https://doi.org/10.1016/j.jclepro.2018.08.110
25. Z. Zhao, Y. Lei, W. Liu, J. Fan, D. Xue, Y. Xue and S. Yin, *Adv. Powder Technol.*, **28**, 3233 (2017); https://doi.org/10.1016/j.apt.2017.09.035
26. N.L. Gavade, S.B. Babar, A.N. Kadam, A.D. Gophane and K.M. Garadkar, *Ind. Eng. Chem. Res.*, **56**, 14489 (2017); https://doi.org/10.1021/acs.iecr.7b03168
27. T.N.T. Thu, N.N. Thi, V.T. Quang, N.K. Hong, T.N. Minh and N.L.T. Hoai, *J. Exp. Nanosci.*, **3**, 226 (2016); https://doi.org/10.1080/17458080.2015.1053541
28. D.I. Cifci and S. Meric, *Glob. NEST J.*, **17**, 653 (2016); https://doi.org/10.30955/gnj.001715
29. J. Lin, Z. Luo, J. Liu and P. Li, *Mater. Sci. Semicond. Process.*, **87**, 24 (2018); https://doi.org/10.1016/j.mssp.2018.07.003
30. S. Siddiqui, F. Zohra and S.A. Chaudhry, *Environ. Res.*, **178**, 108667 (2019); https://doi.org/10.1016/j.envres.2019.108667
31. J. Yin, S. Huang, Z. Jian, Z. Wang and Y. Zhang, *Mater. Sci. Semicond. Process.*, **34**, 198 (2015); https://doi.org/10.1016/j.mssp.2015.02.044
32. H. Liu, D. Yu, T. Sun, H. Du, W. Jiang, Y. Muhammad and L. Huang, *Appl. Surf. Sci.*, **473**, 855 (2019); https://doi.org/10.1016/j.apsusc.2018.12.162
33. J. Liu, X. Liu, J. Li, L. Pan and Z. Sun, *RSC Adv.*, **4**, 38594 (2014); https://doi.org/10.1039/C4RA05389C
34. R. Raliya, C. Avery, S. Chakrabarti and P. Biswas, *Appl. Nanosci.*, **7**, 253 (2017); https://doi.org/10.1007/s13204-017-0565-z
35. C. Lin, Y. Gao, J. Zhang, D. Xue, H. Fang, J. Tian, C. Zhou, C. Zhang, Y. Li and H. Li, *J. Mater. Res.*, **35**, 1307 (2020); https://doi.org/10.1557/jmr.2020.41
36. T. Kim, V.G. Parale, H.N.R. Jung, Y. Kim, Z. Driss, D. Driss, A. Bouabidi, S. Euchy and H.H. Park, *Nanomater.*, **9**, 358 (2019); https://doi.org/10.3390/nano9030358
37. C. Wang, Z. Shi, L. Peng, W. He, B. Li and K. Li, *Surf. Interfaces*, **7**, 116 (2017); https://doi.org/10.1016/j.surfin.2017.03.007